Full Papers
doi.org/10.1002/ejic.202000837

Chemistry Europe
European Chemical Societies Publishing

Revisiting the HKUST-1/S Composite as an Electrode for Li-S Batteries: Inherent Problems That Hinder Its Performance

Jorge de Haro[+],[a] Almudena Benítez[+],[a] Álvaro Caballero,*[a] and Julián Morales*[a]

A composite formed by the HKUST-1 metal-organic framework (MOF) and sulfur (S) was studied as an electrode for Li-S batteries. For preparation, a simple milling procedure in ethanol, to facilitate its homogeneity, was used instead of melt diffusion. Different instrumental techniques were used to characterize the structural, morphological and textural properties of the compound. The results revealed a MOF with a high degree of purity, a high specific surface area and a dual micropore and mesopore system. Although capacity retention is good, losing 0.88 mAh g^{-1} per cycle, capacity values are low, 200 mAh g^{-1} at 100 cycles recorded at C/10 rate. Furthermore, the electrode only gives a moderate electrochemical performance at intermediate current rates. In parallel, a review was carried out of the reported results of this MOF for this application. Although better performances of the HKUST-1 MOF have been published for this application, in some cases, the lack of experimental data to confirm them and serious doubts about the actual content of S in the composite bring the results into question. Only by increasing the additive content, working with low S loading, increasing the measurement voltage window and lowering the current rate can the electrode deliver higher capacities. The inherent problems of this MOF and others with similar properties are indeed their insulating character since the textural properties are adequate for S impregnation and absorption of the polysulfides formed.

Introduction

Among the alkali metal-based batteries, Li-S has one of the highest specific capacities and theoretical energy densities, 1675 mAh g^{-1} and 2500 Wh kg^{-1}, respectively.[1] These values are surpassed by the Li-air battery, but the major design difficulties of this technology hamper its implementation in the short term.[2] Although the challenges for commercial-scale production of Li-S batteries are not so severe, there are still difficulties, among which is the solubility of polysulfides in the electrolyte formed in the early stages of the electrochemical process. These salts can shuttle from the cathode to the anode, causing loss of active material and severe limitations of cell efficiency and cycle life.[3] Several strategies have been used to alleviate this shortcoming, usually based on using S additives. The most common additives are capable of trapping polysulfides in their cavities, an illustrative example is porous carbons,[4–6] or by electrostatic interaction with polar species, an illustrative example is metal oxides.[7–9] Metal-organic frameworks (MOF) are materials that meet both conditions, with a system of pores available to trap polysulfides and the polarity of the M–O bonds favours the electrostatic interaction, showing interesting conditions for energy storage systems.[10–13] This property was confirmed by the pioneering work of Tarascon et al.[14] on MIL-100(Cr) MOF, although the S–MOF composites gave moderate performances. Subsequently, numerous articles have reported expanding this application to other MOFs with different metallic element and ligands.[15–17] Special attention has been paid to the so-called HKUST-1, a MOF of Cu and benzene-1,3,5-tricarboxylic acid (BTC) as the ligand, due to its ease of preparation, a pore system available for S impregnation and unsaturated metal sites to anchor polysulfides.[18] To our knowledge, since the first report in 2013 on applying HKUST-1 in Li-S batteries,[19] at least three more articles have been published, either comparing the behavior with other MOFs,[20] the influence of particle size on cell performance[21] or prepared as a thin film combined with carbon nanotubes.[22]

Table 1 shows some properties of the electrodes prepared using HKUST-1 as the impregnation system for S. The first observation is an evident heterogeneity in the test conditions, both in terms of electrode preparation and electrochemical measurements. When working with carbons as impregnation systems, better conductors than MOFs, the most common electrode composition is 80:10:10. A reduction in composite content is justifiable to increase the carbon black content, but a 60% reduction, as in ref.,[20] is excessive, as is the 40% in ref.,[19] since the advantage of Li-S technology over Li-ion, the greater storage energy, is seriously affected. Furthermore, in the latter case, S loading is too small, below 0.5 mg cm^{-2}, an important parameter that should be indicated in the experimental section of any article on this topic. Another property, the S percentage mixed with the MOF is unsettled. This property is usually quantified using thermogravimetric measurements (TG), taking advantage of the S sublimation between 170–300 °C. In this system, and extendable to other MOFs, the decomposition of the ligand may partly overlap with that of S sublimation, hindering an accurate knowledge of the S content in the

[a] J. de Haro,[+] Dr. A. Benítez,[+] Prof. Á. Caballero, J. Morales
Departamento de Química Inorgánica e Ingeniería Química, Instituto Universitario de Nanoquímica (IUNAN), Facultad de Ciencias, Universidad de Córdoba
Campus de Rabanales, 14071 Córdoba, Spain
E-mail: alvaro.caballero@uco.es
iq1mopaj@uco.es
Homepage: http://www.uco.es/investigacion/ucci/inorganica/
[+] These authors contributed equally to this work.

Table 1. Selected properties of Li-S cells made from HKUST-1/S composites reported in the literature. All composites were prepared by melt diffusion except that of the ref.,[21] which was made from S dissolved in CS_2. The current collectors used were Al foil, except in ref.[22] where carbon paper was used.

S/MOF [%]	Electrode composition[a] [%]	S Loading [mg cm^{-2}]	Long Term Cycling Voltage window [V]	C_i [mAh g^{-1}]	C_f	Cycles	Rate	*Ref.*
40[b]	40:35:25	0.5	3.0–1.0	1498	500	170	C/20	[19]
				1100	210	170[c]		
50[b]	60:30:10	–	2.8–1.8	200	330	40	C/10	[20]
				180	286	300	C/2	
				1050	710	70[d]	C/10	
–	70[e]:20:10	1	2.8–1.7	900	450	50	C/5?	[21]
				1263	911	100[d]	C/5	
				449?[d]	?	?	10 C	
60[b]	75:15:10	–	2.9–1.6	495	230	20	C/10[f]	[22]
				230	200	100	C/5[f]	
40	70:20:10	1.3	2.7–1.8	620	200	100	C/10	This work

[a] Composite: Carbon black: PVDF ratio. [b] Sulfur infiltrated by melt diffusion. [c] Composite prepared without heating. [d] Tabulated values without experimental support in the text. [e] 40% S. [f] The data belongs to the same cell. The first twenty cycles were recorded at C/10 and the next eighty at C/5.

electrode after the composite preparation. We will come back to this idea when discussing the TG results on our composite.

Regarding selecting the conditions of the electrochemical measurements, the voltage window for the galvanic measurements has special relevance since the two stages in which the reaction between S and Li develop are well known and limited between 2.8 and 1.8 V. Pseudo-plateaus are observed in the discharge curve for values below 1.8 V, which are sometimes erroneously attributed to a special type of S confined in the pores. Its origin must be associated with redox reactions that affect the electrolyte, such as the reduction of $LiNO_3$ or another component. This overcapacity raises serious questions about the reliability of electrode performance. Values of over-discharge capacities greater than 40% are obtained by decreasing the voltage from 1.8 to 1.0 V.[21] For somewhat smaller decreases, up to 1.6 V,[21] although the over-discharge values decrease, they are still appreciable, around 10%. Side reactions are also observed when charging the cell to values above 2.8 V, although the overcharge values are pronounced. We have been struck by the fact that in two of the articles reviewed,[20,21] tables appear that collect data on capacity values and cycle number without connection to graphic representations and in contradiction to those set forth precisely in these graphs. In both cases, it is striking that the electrode performance in the tabulated values is better than that deduced from the graphical representations. Without ruling out a lapse from the authors, we do not have a convincing explanation for this divergence in electrode performance between tabulated and graphically represented data.

These previous observations justify the need to delve deeper into the behavior of the HKUST-1 MOF in Li-S batteries, the main objective of this short review. This study may also be of interest for MOFs based on other ligands and/or metals whose thermal instability overlaps with the sublimation temperature of S. If an accurate study of the thermal stability of the MOF is not performed, the TG technique is not the most adequate to calculate the actual S content of the composite and it would be necessary to resort to others that do not present this shortcoming.

Results and Discussion

The MOF crystal structure was examined by XR diffraction, the pattern of which can be indexed in the cubic system with space group symmetry (SG) Fm3m,[23] as shown in Figure 1a, in which

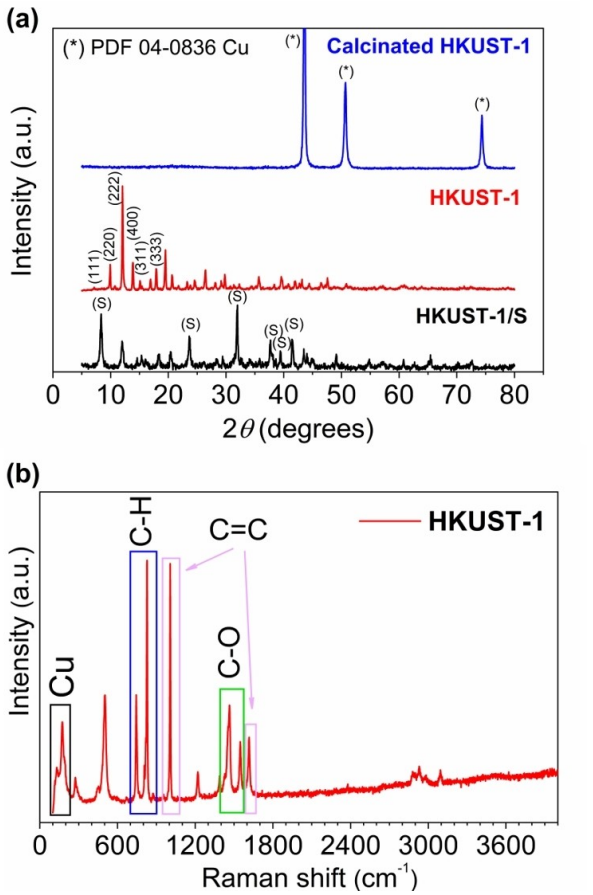

Figure 1. (a) XRD pattern of HKUST-1 MOF (red line), after heating in an O_2 atmosphere (blue line), and sulfur composite (black line). (b) Raman spectrum of HKUST-1.

only the most intense reflections have been indexed. The XRD pattern reflects a satisfactory degree of purity for the synthesized compound.[24,25] Raman spectroscopy was used as a complementary technique for structural characterization. Figure 1b shows the spectrum recorded between 100 and 2000 cm^{-1}. Between 750 and 1800 cm^{-1}, the spectrum is dominated by modes associated with the organic ligand. The bands at 1610 and 1006 cm^{-1} are associated with the vibration modes of the C=C bond in the benzene ring. The peaks at 826 and 740 cm^{-1} are attributed to the out-of-plane bending of the ring C–H bond and out-of-plane bending of the ring, respectively. The doublet at 1550 and 1460 cm^{-1} is assigned to C–O bond symmetric and asymmetric stretching vibrations, respectively. The peaks of the low-frequency region (range 100–600 cm^{-1}) are associated with Cu (II) interaction with ligands and their interpretation is more complex due to the presence of vibrational modes that directly involve the bond between Cu (II) and the ligands. The most outstanding contributions are a doublet with an intense peak at 502 cm^{-1} and a very weak peak at 448 cm^{-1}, a weak, widened beak around 275 cm^{-1} and a complex contribution with two distinct peaks at 193 and 177 cm^{-1}. The good spectrum agreement with that published by other authors[26–28] confirms the high degree of purity of the synthesized compound.

The SEM image of Figure 2a shows the octahedral shape of the compound's crystals, reflecting its structural framework.[29] The size ranges from approximately 15 to 20 μm. The size is larger than when the compound synthesis is performed without hydrothermal treatment.[29]

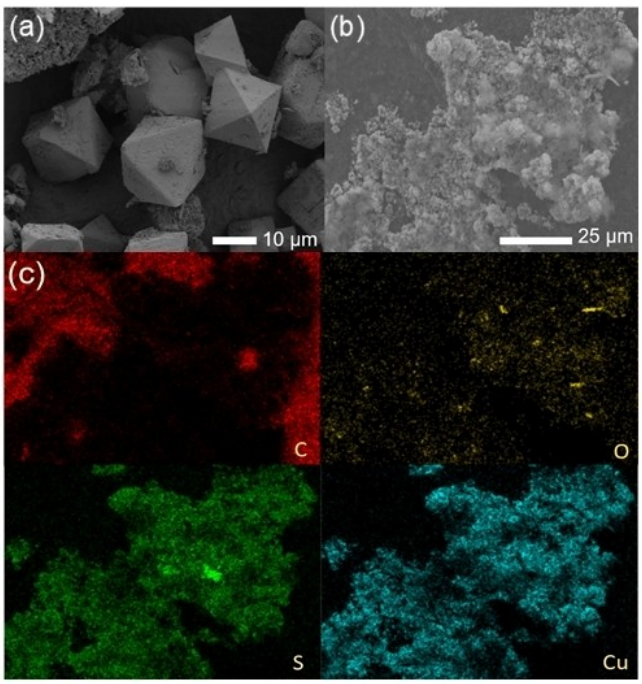

Figure 2. SEM images of HKUST-1 (a) and sulfur composite (b). (c) Mapping of the elements C, O, S and Cu obtained from the EDS spectrum of SEM image b.

The surface area and pore structure of a material capable of acting as an electrode in Li-S cells play important roles in its electrochemical behavior. These properties were determined from N_2 adsorption measurements. The adsorption/desorption isotherm of the compound is shown in Figure 3a. Up to relative pressures $P/P_0 = 0.4$, the shape of the adsorption isotherm conforms to Type I in the BDDT classification, typical of microporous solids. The steepest increase in adsorption volume at higher relative pressures and the hysteresis cycle observed in the desorption isotherm reveal a change in the shape of the Type IV isotherm, typical of mesoporous solids. Therefore, the shape of the isotherm suggests that the compound has a dual system of micropores and mesopores. Table 2 shows the values of the textural parameters obtained from evaluating the adsorption data. Although the calculated value for the specific surface S_{BET}, 825 $m^2 g^{-1}$, is intermediate to that measured by other authors, 692[18] and 1140 $m^2 g^{-1}$,[30] the total pore volume (V_T) is greater, 0.505 $cm^3 g^{-1}$, compared to 0.333 and 0.420 $cm^3 g^{-1}$ in references[18] and,[30] respectively. The surface

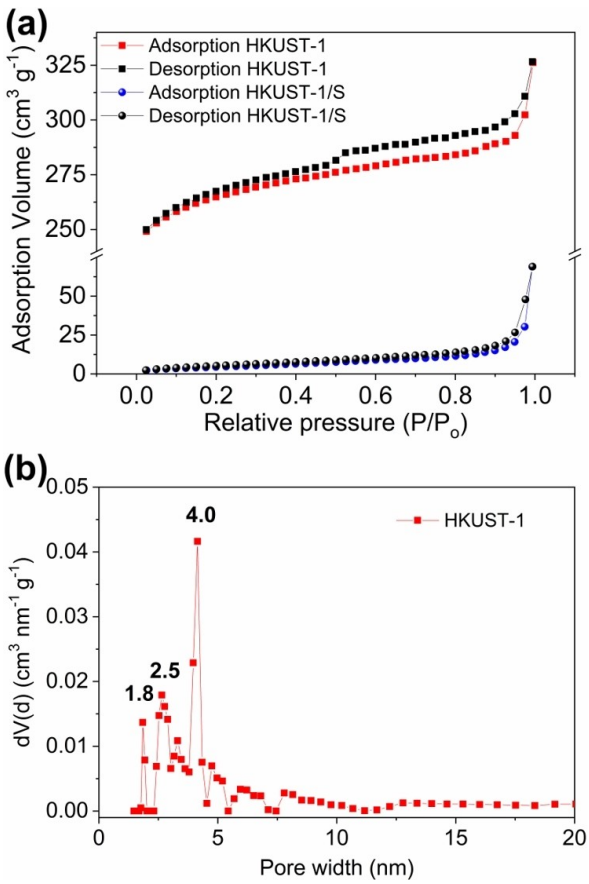

Figure 3. (a) N_2 adsorption/desorption isotherms and (b) Pore size distribution obtained from the DFT model for HKUST-1.

Table 2. Textural parameters obtained from the N_2 adsorption isotherms.

Sample	S_{BET} [$m^2 g^{-1}$]	S_{micro} [$m^2 g^{-1}$]	V_T [$cm^3 g^{-1}$]	V_{micro} [$cm^3 g^{-1}$]
HKUST-1	825	730	0.505	0.368
HKUST-1/S	18	–	0.107	–

values and the volume adsorbed by the micropores (V_{micro}) reach high values, 88 and 72%, respectively, values that demonstrate the importance of the compound's micropore system. The presence of S causes significant changes in the textural properties of the composite. The shape of the nitrogen adsorption-desorption isotherm shifts to Type II, characteristic of non-porous materials, Figure 3a (the small hysteresis loop can be associated to an interparticle mesopore system[31]). Furthermore, a sharp drop in the adsorbed volume values is observed and the surface area and pore volume significantly decrease to 18 $m^2 g^{-1}$ and 0.107 $cm^3 g^{-1}$, respectively. This is the usual behavior observed when the material is impregnated with S.[32,33] Figure 3b shows the analysis of the pore size distribution for HKUST-1 carried out using the density functional theory (DFT) model. Four peaks appear in this plot for sizes less than 5 nm, three well defined with values of 1.8, 2.5 and 4.0 nm, which confirm the dual nature of the compound in terms of its pore system.

To improve the compound characterization, its weight loss curve was recorded in a dynamic N_2 and O_2 atmosphere. In both conditions, the thermogravimetric curves, Figure 4, show two weight losses. The first begins at room temperature and ends at temperatures slightly above 100 °C. The low temperature suggests water loss, in good agreement with the compound's ease of absorbing water from the air. The calculated loss is around 26.4% in N_2 and 28.5% in O_2. Under an N_2 atmosphere, the second stage of weight loss starts at around 200 °C and continues up to 500 °C, the measured temperature limit. The total loss is 32.2% and is more pronounced between 300 and 400 °C. In O_2 atmosphere, this stage also begins at around 200 °C, but starting at 300 °C, the weight remains virtually constant. The weight loss is greater by 41.4%. The compound decomposition in O_2 atmosphere was studied by Lin et al..[35] The amount of water lost in the first stage is somewhat lower, around 21%. These data, together with the difference in weight loss found in our measurements, are consistent with the easiness of compound hydration. The weight loss measured in the second stage, around 42%, is like that observed in our work. The proposed formula for the synthesized MOF was $Cu_3[(BTC)_2(H_2O)_3]\cdot nH_2O$. The loss of the three coordination H_2O molecules would mean a loss of around 8.5%. Therefore, the rest would correspond to the H_2O of hydration, not directly bound to Cu^{2+} ions. The problem of this compound is the virtual equivalence in the interaction forces of both types of water molecules within the structural framework of the Cu-BTC system, hence, they cannot be differentiated using thermal measurements.

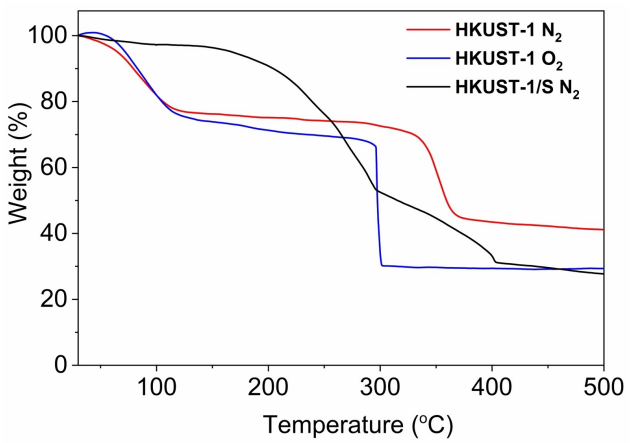

Figure 4. TG curves of HKUST-1 recorded in N_2 and O_2, and the HKUST-1/S composite in N_2 atmosphere.

Lin et al.[35] identified CuO formation as an expected phase resulting from decomposition in O_2 atmosphere. The decomposition reaction in a nitrogen atmosphere should lead to different phases. We have not found data that identify the phases formed in an N_2 atmosphere, so the XRD pattern of the resulting product after heating to 500 °C was recorded, Figure 1a. The pattern demonstrates the formation of Cu metal (Pattern Diffraction File, PDF #04-0836). Oxidized phases such as CuO, expected according to the initial valence of Cu in the compound structure, and Cu_2O, are not detected. Neither is the C formation clearly detected unless the pattern scale is expanded. Under these conditions, a very weak widened peak is observed in the region in which the (002) plane of graphite should appear, between 20 and 30° 2θ, depending on the degree of crystallinity.[36] Consequently, the carbon formed is virtually amorphous. The formation of Cu would be a consequence of reducing gases release (CO, CH_4 …) or of C itself formed in the pyrolysis process. In summary, the reactions that would take place when heating the compound to 500 °C would be:

$$O_2\ \text{atmosphere}: \ Cu_3[(BTC)_2(H_2O)_3]\cdot nH_2O(s) + O_2(g) \rightarrow CuO(s) + (n+3)\ H_2O(g) + CO_2(g) \quad (1)$$

$$N_2\ \text{atmosphere}: \ Cu_3[(BTC)_2(H_2O)_3]\cdot nH_2O(s) + N_2(g) \rightarrow Cu(s) + (n+3)\ H_2O(g) + C\ (s, \text{amorphous}) + \text{unidentified gases} \quad (2)$$

The stability of the MOF increases by about 50 °C when heating is carried out in an N_2 atmosphere.

The XRD pattern of the HKUST-1/S composite is shown in Figure 1a. The main peaks of the MOF are maintained, and the reflections of S appear in its orthorhombic structure allotropic form. These results show that the wet grinding process barely affects the structure of both components. The grinding process affects the particle morphology more, with a tendency to break and lose the octahedral shape, as shown in Figure 2b. The mapping of C, O, Cu and S obtained from the EDS spectrum is shown in Figure 2c. From these images, it is worth noting the homogeneous distribution of S. The actual S content of the composite was obtained from its TG curve in N_2 atmosphere, Figure 4. Compared with the MOF curve, several differences should be highlighted, namely: (i) a lower H_2O content, around 2.3%, just one molecule of water of hydration and (ii) a weight loss of around 42% between 150–300 °C, assigned to S sublimation.[36] Between 300 and 500 °C, the shape is identical to that described for the MOF with a weight loss of around

30.8%. The S content is below 51%, calculated from the pore volume by the formula W_S (%) = $(\rho_S \cdot V/(\rho_S \cdot V + 1) \times 100$, where ρ_S is the density of sulfur ($\simeq$2.07 g cm^{-3}) and V the pore volume of the carbon matrix (0.505 cm^3 g^{-1}).[37] Consequently, there are still empty cavities available for the mobility of the species formed in the electrochemical reaction.

As mentioned in the Introduction, confirming the S content of the composite was done by analyzing the thermogravimetric measurements recorded in an N_2 atmosphere (Figure 4). MOFs are compounds with low thermal stability due to the low pyrolysis temperature of the organic ligand, a temperature that can overlap with the sublimation of the composite S, which generally takes place between 150–300 °C; hence the need for a comparative study between the thermal stability of the pristine MOF and the composite. Table 3 shows weight loss values at different temperatures of the HKUST-1/S system reported in the literature along with those obtained in this work. This dual thermal study was performed in all of them, except for Mao et al.,[21] which only included the TG curve of the composite. The composite loses 40% of weight up to 265 °C, assigned to the S, followed by 14.7% assigned to the MOF. Since pristine MOF loses around 48%, the results of the thermal study raise serious doubts about the actual composition of the composite. The composite MOF/S described by Zhou et al.[20] was prepared with a 1:1 weight ratio, so it should lose 50% assignable to S. A 50% weight loss was reached at about 380 °C. Considering that the composite loses 65.5% of its weight, the MOF would only lose 15.5%, far from the 25% that should be observed since pure MOF loses more than 50%. Consequently, the weight loss values differ markedly from the composition used in the preparation and raise serious doubts about the actual capacity values of the electrode. A similar problem was shown by the results published by Baumann et al..[22] In this case, the TG curve is described in five stages associated with the loss of solvent adsorbed physically (< 120 °C) and chemically (120–200 °C), S adsorbed physically (190–180 °C) and chemically (280–310 °C), and MOF decomposition (310–400 °C). This model is based on a so-called "coordination modulation method" proposed by Wang et al.[38] to explain the different morphologies of the HKUST-1 when three types of modulators are used, sodium formate, sodium acetate and triethylamine. These compounds are very different from the solvents (H_2O) or S present in the composite, so the analogy is highly questionable. As for the S content, around 40%, we do not understand the phrase which appears in the article "*a typical S weight loading of ~65%, as determined by thermogravimetric analysis* (Table S4)"; hence, the capacity values collected in Table 1 are misleading. When the processes of S sublimation and MOF decomposition occur at different temperatures, the thermogravimetric technique is indeed appropriate to quantify the actual content of S in the composite. This requirement is met in the TG curves recorded in our work, (Figure 4) and that of Wang et al..[19] In the latter, the percentage of S, 40%, coincides with that used to prepare the composite. In our composite, the S used was also 40%. The weight loss is slightly higher, 42.5%, either because it is somewhat hydrated or when it is ground and recovered it from the jar, the MOF/S ratio may have changed slightly. As expected in both cases, the calculated MOF weight loss is consistent with that obtained from the TG curve (see Table 1).

The cyclic voltammetry (CV) curves of the HKUST-1/S composite recorded at 0.05 mV s^{-1} a scan rate in the 1.7 to 2.7 V range are shown in Figure 5a. Two asymmetric reduction peaks at 2.3 and 2.03 V, the latter very wide, are assigned to the various stages of sulfur reduction. The first peak is generally attributed to the opening of the S_8 ring followed by the formation of long-chain polysulfides (Li_2S_x, $4 \leq x \leq 8$) and the second is associated with a greater reduction of these polysulfides to short-chain polysulfides (Li_2S_2 and Li_2S).[39,40] The oxidation process in the Li-S battery also occurs in two stages. The anode sweep shows a broad, asymmetric peak centred at ca. 2.4 V, attributed to the observed inverse reactions on the reduction curve. The slowness of these reactions causes a polarization, a significant overlap of both stages and, as a result, the appearance of a widened and asymmetric peak. In the

Table 3. Weight loss values (in %) of HKUST-1 and HKUST-1/S composite reported in the literature. The values found in this work have also been included for comparison.

Temperature range °C	Samples MOF	MOF/S	Reference
25–150	23.3	2.3	This work
150–300	–	42.5	
300–500	34.1	24.5; 25.3[a]	
200–330	2.7	40.0	[19]
330–600	44.6	27.9; 28.3[a]	
150–280	–	27	[20]
280–600	50.5	38.5	
140–265	–	40.0	[21]
265–500	–	14.7	
25–200	15	–	[22]
200–400	48	–	
25–190	–	12	
190–310 (S_{phys}, S_{chem})	–	39.5	
310–340	–	18.6	

[a] Value calculated considering the thermal behavior of the pristine MOF.

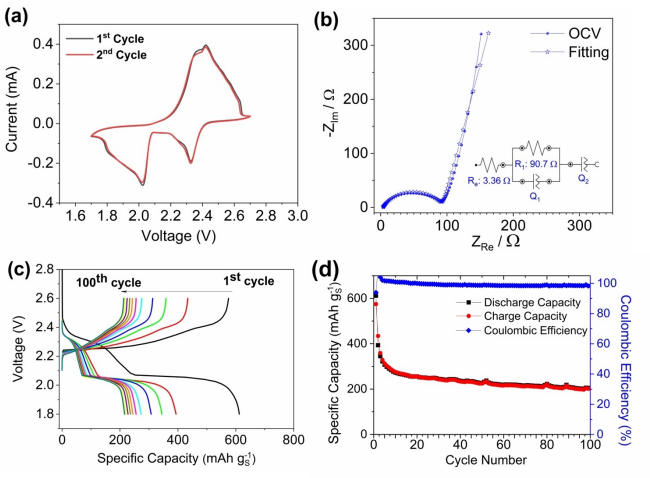

Figure 5. Cyclic voltammetry curves of HKUST-1/S composite recorded at 0.05 mV s^{-1} (a) and EIS measurements at open circuit voltage (OCV) (b). Galvanostatic curves recorded at C/10 (c). Variation in the discharge capacity and coulombic efficiency as a function of the number of cycles (d).

second cycle, the shape of the curves undergoes little significant change, proof of the reversibility of electrochemical reactions. Figure 5b shows the Nyquist plot of the impedance spectroscopy test performed at the open-circuit voltage (OCV) using HKUST-1/S electrode. The behavior of the cell is associated with an equivalent circuit of the type $R_e(R_1Q_1)Q_2$ consisting of an electrolyte resistance R_e (3.36 Ω) at high frequency in series with the R_1Q_1 element (R_1 = 90.7 Ω). In the medium-high frequency range the semicircle is assigned to the resistance and capacitance of electrode/electrolyte interphase, including the solid electrolyte interphase (SEI) layer formed at the electrodes surface. The last element in the low-frequency region (Q_2) can actually account for the diffusion of lithium ions at the electrode/electrolyte interphase, being a constant phase element (CPE) that is similar to an ideal capacitive element but has an angle absolute phase of less than 90°. The Nyquist plot resembles the one published by Mao et al.[21] for a S/HKUST-1 with a S content similar to ours. The expected R_1 value would be around 90 Ω, comparable to the one calculated here.

The galvanostatic charge and discharge curves recorded at 0.1 C (1 C = 1675 mA g^{-1}) in the 2.6–1.8 V potential range are shown in Figure 5c for some of the measured cycles. All discharge curves exhibit two typical pseudo-plateaus, consistent with the two-stage mechanism of the electrochemical Li-S reaction reflected at the two peaks of the voltammetric curves (Figure 5a). A sharp drop in potential is observed on moving from the first to the second due to the slow formation of Li_2S_2/Li_2S, the reason for the separation between the two peaks of the cathodic scan of the CV curve.[42,43] For the same reason, the charging process begins with a strong polarization that decreases the difference in potential of the two reverse processes, and therefore, the two peaks in the anode scan are not well resolved (Figure 5a). The values of the capacity supplied by the cell as a function of the number of cycles are shown in Figure 5d. The value of the first discharge was 620 mAh g^{-1}, less than 40% of theoretical. Several causes are possible, from the insulating nature of the compound its conductivity is around 10^{-8} S cm^{-1}[43] much lower than that of carbon black 10^{-1} S cm^{-1},[44] to its ease of hydration. In fact, in the first study carried out on using MOF as an S additive for an electrode for Li-S batteries, the so-called MIL-100Cr,[14] obtained from a Cr (III) salt and benzene-1, 3, 5-tricarboxylic acid, to achieve an acceptable electrochemical response, it was necessary: (i) to degas the MOF at 170 °C; (ii) to perform the composite formation with molten S at 155 °C; (iii) add 50% carbon black (CB) and (iv) set the voltage window at 1.0–3.0 V, and resulted in the presence of especially perceptible side reactions in the discharge process. In the second cycle, Figure 5d, the discharge capacity decreased significantly and was around 400 mAh g^{-1}. In subsequent cycles, the decrease in capacity was moderated and in cycle 10, it was 280 mAh g^{-1}. At 100 cycles the capacity was 200 mAh g^{-1}, showing a clear improvement in capacity retention (loss of 0.88 mAh g^{-1} per cycle). The marked drop in capacity when passing from the first to the second cycle is reflected in a strong polarization between the respective discharge curves (see Figure 5c); once the cell is in operation, it requires additional time to stabilize and the electrolyte is distributed homogeneously in the active mass of the cathode. From cycle 10, the cell stabilizes, as do both the polarization between the curves and the loss of capacity. Similar reasoning can be applied to charge curves. In fact, the coulombic efficiency, the ratio between the value of the charge and the discharge, deviates from 100% in the first cycles. The trend is to approach 100% after the first cycles, indicative behavior that the "shuttle" effect has little impact. The electrochemical properties in Li-S batteries of this HKUST-1 MOF are somewhat better than that of the Cr-based MOF in ref.,[14] with CB values of 12.5%, equal current rate, 0.1 C, but greater voltage window, between 1 and 3 V. The discharge capacity of this electrode in the first cycle was 500 mAh g^{-1}; in the second cycle, it dropped to 370 mAh g^{-1} and in the last measured cycle, 62, 160 mAh g^{-1}, showing worse capacity retention (loss of capacity per cycle 3.44 mAh g^{-1}).

Measuring the electrochemical properties was completed with the study of the electrode's rate capability. The current densities were progressively increased starting at C/10 and continuing at C/8, C/5, C/2 and 1 C. The last stage was to return to the initial value, 0.1 C to analyze the cell's recoverability. The discharge/charge curve of the first cycle for each current density is shown in Figure 6a. The profiles are like those described in Figure 5c. It is worth noting the increase in polarization between the charge and discharge curves with increasing current density is due to the sluggish reaction between Li and S. This obstacle leads to a decrease in capacity with increasing current density. The capacity values at the

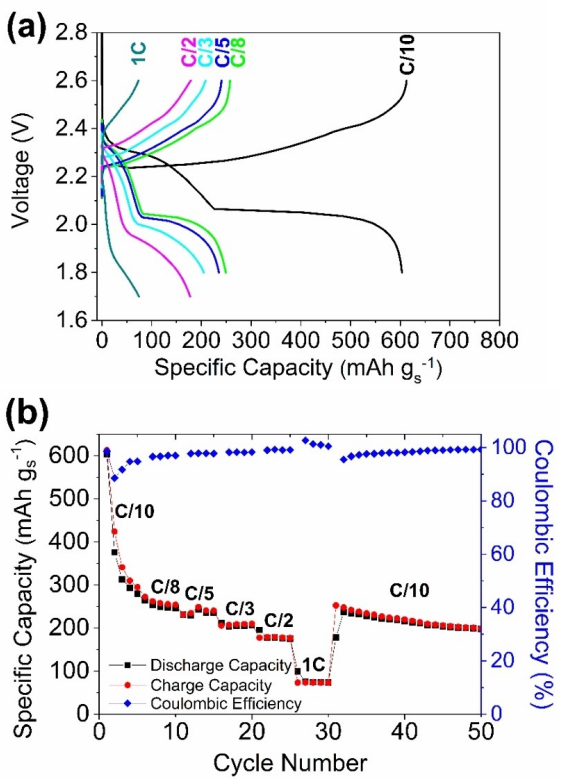

Figure 6. (a) Galvanostatic curves recorded at different current density for HKUST-1/S composite as the cathode in Li-S cells. (b) Rate performance.

different current densities used are shown in Figure 6b. The five cycles recorded at C/10 served to stabilize the cell. The average capacity values for the remaining current densities were 250, 230, 200, 170 and 70 mAh g^{-1} at C/8, C/5, C/3, C/2 and 1 C, respectively. Decreasing capacity with increasing current density is the expected behavior. For this electrode, numerical values show that the cell responds reasonably well for moderate current densities, up to C/2, but the response is less satisfactory for higher densities. However, despite this drawback, when cycling back to C/10, the cell delivers initial-like values with high capacity retention. Regarding the values of the coulombic efficiency, the behavior is like that for the data on prolonged cycling, Figure 5d. For the different current densities, the tendency is to reach values close to 100 % as the number of cycles increases.

Conclusions

Although it is difficult to establish comparisons between the performance of our electrode and those published by other authors, in Table 1, given the differences in the composition and preparation of the composite and in the measurement conditions, some observations can be made on the advantages and disadvantages of using HKUST-1 MOF as a Li-S battery electrode compared to other MOFs with similar properties. To obtain reasonably high values of capacity it is required to: (i) decrease S content in the electrode and increase the CB to improve conductivity; this option negatively affects S loading; (ii) use low current densities, and (iii) increase the potential window, thereby enhancing side reactions that would affect the electrolyte stability. This was the strategy followed in the first study of this material for this application.[19] Although in later reports, the electrode performance was improved, increasing the content of S and the tendency to reduce the potential window;[20–22] however, experimental measurements to confirm this are lacking. In addition, serious doubts arise about the actual S content since it was extracted from thermogravimetric measurements in which the weight loss of the composite overlaps with the sublimation of S. Although our capacity values are lower than those obtained by Wang et al.,[19] the most reliable of those reviewed in Table 1, the amount of S in the electrode is higher, more than double; double the current density used and the voltage window, appropriate so that the only observable electrochemical reaction is between Li and S. In addition, the melt diffusion method was not used for S impregnation in favour of simply ball milling under wet conditions (ethanol). Although the HKUST-1 MOF, in addition to its ease of preparation, has a high porosity and specific surface area suitable for impregnating S and trapping polysulfides, its insulating character, as occurs with S, considerably hinders the mobility of charge carriers and does not enhance the electrochemical reaction kinetics. The result is a low performance for this type of battery. For other MOFs with a similar problem, it is foreseeable that they will not be ideal for application in Li-S batteries, although a revision would be necessary to confirm this opinion.

Experimental Section

HKUST-1 preparation

3.6 mmol (869.62 mg) of $Cu(NO_3)_2 \cdot 3H_2O$ (Sigma-Aldrich) were dissolved in 18 mL distilled water and 4 mmol (840.56 mg) of 1,3,5-benzenetricarboxylic acid (Sigma-Aldrich) were dissolved in 18 mL of ethanol. These solutions were mixed with stirring for 30 min. The resulting solution was transferred to a 100 mL Teflon-coated stainless-steel autoclave and heated at 120 °C for 12 hours.[45] The suspension was washed three times with water and once with ethanol and centrifuged at 3500 rpm for 15 min. The resulting solid was dried in a vacuum oven at 80 °C overnight. Under these conditions, the compound acquires a dark blue colour.

HKUST-1/S composite preparation

135 mg of HKUST-1 MOF were mixed with 90 mg of S. The mixture was prepared in an agate mortar and was subsequently ground in a planetary ball mill (Restch PM100, Retsch GmbH, Haan, Germany) at 300 rpm for 3 hours and changes of rotation every 15 min. The wet milling process was carried out using ethanol as a dispersant agent.

Electrode preparation

The positive electrodes were prepared by mixing 70 wt.% of the as-prepared HKUST-1/S composite, 20 wt.% of the conductive agent (Super P carbon, Timcal), and 10 wt.% of polyvinylidene fluoride (PVDF 6020, Solvay) as a binder in N-methyl-2-pyrrolidone (NMP, Sigma-Aldrich) in a manual mortar until a homogeneous slurry was formed. Then, the slurry was cast on Al foil (50 μm thickness) using a doctor blade collector for the carbon-sulfur composites of Li-S cells.[46] After drying, the electrodes were punched into 13 mm diameter discs (1.33 cm^2 geometric surface). The cathode discs were then further dried in a vacuum oven (Buchi, Flawil, Switzerland) at 45 °C for 2 h. The S loading was ca. 1.3 mg cm^{-2}. The diagram shown in Scheme 1 summarizes the sequential steps used for preparing the Li-S cells based on HKUST-1/S composite.

Material characterization

The structural and textural properties of the as-fabricated materials were analyzed by different characterization techniques. X-ray diffraction (XRD) was used to study the structures and the patterns were obtained through a Bruker D8 Advance diffractometer equipped with a Cu Kα source (λ = 1.5406 Å) at 40 kV and 40 mA over the 5 to 80° 2θ range at a 1.05 s per step rate with a 0.04° step size. Pattern Diffraction File database was used for the identification of crystalline phases. Raman spectra were recorded with a confocal Raman spectrometer (Raman Renishaw; InVia Raman Microscope). A frequency-doubled Nd:YAG laser at 532 nm (second harmonic generation) was used for excitation. Thermogravimetric analysis was carried out using a Mettler Toledo-TGA/DSC with a heating rate of 5 °C min^{-1} under an N_2 or O_2 atmosphere from 30 to 800 °C. Sample morphologies were investigated using a JEOL JSM-7800F scanning electron microscope (SEM). The SEM was coupled to a microanalysis system for obtaining the energy-dispersive X-ray spectra (EDS). Nitrogen adsorption-desorption isotherms were obtained on an Autosorb iQ/ASiQwin (Quantachrome Instruments, Anton Paar GmbH, Graz, Austria). Specific surface areas were determined by the Brunauer-Emmett-Teller (BET) method. Total pore volumes (V_T) were determined according to the amount adsorbed at a relative pressure (P/P_0) of 0.995. Pore size distributions were calculated using the density functional theory (DFT) method applied to the adsorption branch of the isotherms. The

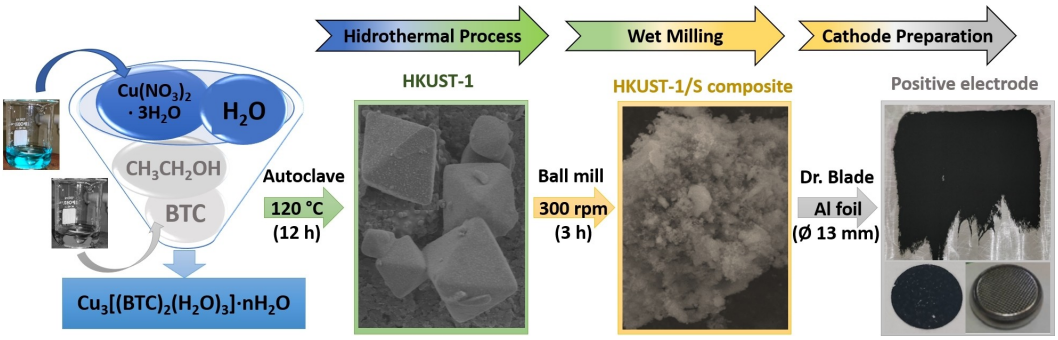

Scheme 1. Schematic diagram for the preparation of HKUST-1/S composite as a cathode for Li-S batteries.

micropore surface area and volume were estimated using the t-plot method.

Electrochemical measurements

The electrochemical behavior of the working electrode was studied in coin-type CR2032 cells, assembled inside an Ar-filled glove box (M-Braun 150, M-Braun, Garching, Germany). Lithium metal foil (Li, Gelon Lib, Qingdao, China, 15.6 mm diameter and 0.25 mm thick) served as the counter and reference electrodes. Polyethene membrane (PE, 25 μm thick, Celgard 2400, Charlotte, NC, USA) was used as a separator. The electrolyte was 1 M LiTFSI with 0.4 M $LiNO_3$ on a 1:1 (v:v) solution of DME:DOL. Cyclic voltammetry (CV) curves and electrochemical impedance spectroscopy (EIS) were recorded using an Autolab PGSTAT-204 (Metrohm, Herisau, Switzerland). Impedance spectrum was recorded at the open circuit voltage (OCV) condition, by applying an alternative voltage signal of 10 mV amplitude within the 500 kHz to 0.1 Hz frequency range. Galvanostatic cycling tests were performed on an Arbin BT2143 (Arbin Instruments, College Station, USA) within the 1.8–2.6 V potential window.

Acknowledgements

This research was funded by Ministerio de Economía y Competitividad (Project MAT2017-87541-R) and Junta de Andalucía (Group FQM-175). A. Benítez thanks the financial support from Cordoba University (Plan Propio de Investigación 2019; Sub. 2.4.). The authors wish to acknowledge the technical staff from the Instituto Universitario de Nanoquímica (IUNAN) and Servicio Central de Apoyo a la Investigación (SCAI) of Cordoba University.

Conflict of Interest

The authors declare no conflict of interest.

Keywords: HKUST-1 · Li-S batteries · Metal-organic frameworks · Pore systems · Sulfur

[1] A. Manthiram, Y. Fu, S.-H. Chung, C. Zu, Y.-S. Su, *Chem. Rev.* **2014**, *114*, 11751–11787.
[2] A. Manthiram, S.-H. Chung, C. Zu, *Adv. Mater.* **2015**, *27*, 1980–2006.
[3] Y.-X. Yin, S. Xin, Y.-G. Guo, L.-J. Wan, *Angew. Chem. Int. Ed.* **2013**, *52*, 13186–13200; *Angew. Chem.* **2013**, *125*, 13426–13441.
[4] S. Li, B. Jin, X. Zhai, H. Li, Q. Jiang, *ChemistrySelect* **2018**, *3*, 2245–2260.
[5] Z. Li, L. Wang, Y. Li, Y. Feng, W. Feng, *Compos. Sci. Technol.* **2019**, *179*, 10–40.
[6] A. Benítez, D. Di Lecce, G. A. Elia, Á. Caballero, J. Morales, J. Hassoun, *ChemSusChem* **2018**, *11*, 1512–1520.
[7] X. Liang, C. Y. Kwok, F. Lodi-Marzano, Q. Pang, M. Cuisinier, H. Huang, C. J. Hart, D. Houtarde, K. Kaup, H. Sommer, T. Brezesinski, J. Janek, L. F. Nazar, *Adv. Energy Mater.* **2016**, *6*, DOI 10.1002/aenm.201670039.
[8] J. Li, M. Zhu, P. Hu, X. Wang, L. Zhang, M. Li, *Eur. J. Inorg. Chem.* **2017**, *2017*, 3248–3252.
[9] Y. Ning, B. Wang, F. Jin, J. Yang, J. Zhang, H. Luo, F. Wu, Z. Zhang, H. Zhang, Y. Zhou, D. Wang, *J. Alloys Compd.* **2020**, *838*, 155504.
[10] Z. Liang, R. Zhao, T. Qiu, R. Zou, Q. Xu, *EnergyChem* **2019**, *1*, 100001.
[11] K.-B. Wang, Q. Xun, Q. Zhang, *EnergyChem* **2020**, *2*, 100025.
[12] X. Li, X. Yang, H. Xue, H. Pang, Q. Xu, *EnergyChem* **2020**, *2*, 100027.
[13] S. Zheng, Q. Li, H. Xue, H. Pang, Q. Xu, *Natl. Sci. Rev.* **2020**, *7*, 305–314.
[14] R. Demir-Cakan, M. Morcrette, F. Nouar, C. Davoisne, T. Devic, D. Gonbeau, R. Dominko, C. Serre, G. Férey, J.-M. Tarascon, *J. Am. Chem. Soc.* **2011**, *133*, 16154–16160.
[15] Y. Zheng, S. Zheng, H. Xue, H. Pang, *J. Mater. Chem. A* **2019**, *7*, 3469–3491.
[16] S. Kuyuldar, D. T. Genna, C. Burda, *J. Mater. Chem. A* **2019**, *7*, 21545–21576.
[17] W. Bao, Z. Zhang, Y. Qu, C. Zhou, X. Wang, J. Li, *J. Alloys Compd.* **2014**, *582*, 334–340.
[18] S. S. Y. Chui, *Science* **1999**, *283*, 1148–1150.
[19] Z. Wang, X. Li, Y. Cui, Y. Yang, H. Pan, Z. Wang, C. Wu, B. Chen, G. Qian, *Cryst. Growth Des.* **2013**, *13*, 5116–5120.
[20] J. Zhou, R. Li, X. Fan, Y. Chen, R. Han, W. Li, J. Zheng, B. Wang, X. Li, *Energy Environ. Sci.* **2014**, *7*, 2715.
[21] Y. Mao, G. Li, Y. Guo, Z. Li, C. Liang, X. Peng, Z. Lin, *Nat. Commun.* **2017**, *8*, 14628.
[22] A. E. Baumann, G. E. Aversa, A. Roy, M. L. Falk, N. M. Bedford, V. S. Thoi, *J. Mater. Chem. A* **2018**, *6*, 4811–4821.
[23] L. D. O'Neill, H. Zhang, D. Bradshaw, *J. Mater. Chem.* **2010**, *20*, 5720.
[24] S. Bai, X. Liu, K. Zhu, S. Wu, H. Zhou, *Nat. Energy* **2016**, *1*, 16094.
[25] P. Liao, H. Fang, J. Zhang, Y. Hu, L. Chen, C.-Y. Su, *Eur. J. Inorg. Chem.* **2017**, *2017*, 2580–2584.
[26] C. Prestipino, L. Regli, J. G. Vitillo, F. Bonino, A. Damin, C. Lamberti, A. Zecchina, P. L. Solari, K. O. Kongshaug, S. Bordiga, *Chem. Mater.* **2006**, *18*, 1337–1346.
[27] M. D. Allendorf, R. J. T. Houk, L. Andruszkiewicz, A. A. Talin, J. Pikarsky, A. Choudhury, K. A. Gall, P. J. Hesketh, *J. Am. Chem. Soc.* **2008**, *130*, 14404–14405.
[28] S. D. Worrall, M. A. Bissett, P. I. Hill, A. P. Rooney, S. J. Haigh, M. P. Attfield, R. A. W. Dryfe, *Electrochim. Acta* **2016**, *222*, 361–369.
[29] G. G. da Silva, F. L. A. Machado, S. A. Junior, E. Padrón-Hernández, *J. Solid State Chem.* **2017**, *253*, 1–5.
[30] K.-Y. Andrew Lin, Y.-T. Hsieh, *J. Inst. Chem.* **2015**, *50*, 223–228.
[31] J. M. Morales, A. Moragues, J. El Haskouri, C. Guillem, J. Latorre, S. Murcia-Mascarós, A. Beltrán, D. Beltrán, P. Amorós, *ChemPlusChem* **2015**, *80*, 1014–1028.
[32] N. Moreno, M. Agostini, A. Caballero, J. Morales, J. Hassoun, *Chem. Commun.* **2015**, *51*, 14540–14542.

[33] N. Moreno, A. Caballero, L. Hernán, J. Morales, J. Canales-Vázquez, *Phys. Chem. Chem. Phys.* **2014**, *16*, 17332–17340.
[34] K.-S. Lin, A. K. Adhikari, C.-N. Ku, C.-L. Chiang, H. Kuo, *Int. J. Hydrogen Energy* **2012**, *37*, 13865–13871.
[35] F. J. Soler-Piña, C. Hernández-Rentero, A. Caballero, J. Morales, E. Rodríguez-Castellón, J. Canales-Vázquez, *Nano Res.* **2020**, *13*, 86–94.
[36] F. Luna-Lama, C. Hernández-Rentero, A. Caballero, J. Morales, *Electrochim. Acta* **2018**, *292*, 522–531.
[37] C. Hernández-Rentero, R. Córdoba, N. Moreno, A. Caballero, J. Morales, M. Olivares-Marín, V. Gómez-Serrano, *Nano Res.* **2018**, *11*, 89–100.
[38] F. Wang, H. Guo, Y. Chai, Y. Li, C. Liu, *Microporous Mesoporous Mater.* **2013**, *173*, 181–188.
[39] Y. J. Li, J. M. Fan, M. Sen Zheng, Q. F. Dong, *Energy Environ. Sci.* **2016**, DOI 10.1039/c6ee00104a.
[40] N. Moreno, A. Caballero, J. Morales, M. Agostini, J. Hassoun, *Mater. Chem. Phys.* **2016**, *180*, 82–88.
[41] W. Zhu, A. Paolella, C.-S. Kim, D. Liu, Z. Feng, C. Gagnon, J. Trottier, A. Vijh, A. Guerfi, A. Mauger, C. M. Julien, M. Armand, K. Zaghib, *Sustain. Energy Fuels* **2017**, *1*, 737–747.
[42] A. Paolella, W. Zhu, H. Marceau, C. Kim, Z. Feng, D. Liu, C. Gagnon, J. Trottier, G. Abdelbast, P. Hovington, A. Vijh, G. P. Demopoulos, M. Armand, K. Zaghib, *J. Power Sources* **2016**, *325*, 641–645.
[43] Z. Li, Y. Guo, X. Wang, W. Ying, D. Chen, X. Ma, X. Zhao, X. Peng, *Chem. Commun.* **2018**, *54*, 13865–13868.
[44] D. Pantea, H. Darmstadt, S. Kaliaguine, C. Roy, *Appl. Surf. Sci.* **2003**, *217*, 181–193.
[45] X. Gao, G. Zhu, X. Zhang, T. Hu, *Microporous Mesoporous Mater.* **2019**, *273*, 156–162.
[46] A. Benítez, Á. Caballero, E. Rodríguez-Castellón, J. Morales, J. Hassoun, *ChemistrySelect* **2018**, *3*, 10371–10377.

Manuscript received: September 5, 2020
Revised manuscript received: October 28, 2020
Accepted manuscript online: October 29, 2020

FULL PAPERS

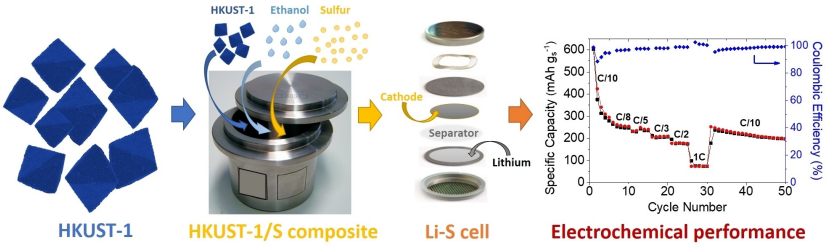

J. de Haro, Dr. A. Benítez, Prof. Á. Caballero, J. Morales**

A metal organic framework has been prepared by a hydrothermal heating process at 120 °C. This material shows high degree of purity, an appreciable specific surface area and pore volume and, a dual system of micro- and mesopores. MOF/S composite were prepared through a simple process of ball milling with ethanol. These properties are beneficial for its performance as a cathode in Li-S batteries.

Caballero, Morales and co-workers prepared a pure, high-surface-area metal organic framework with good performance as cathode in Li-S batteries @Univcordoba @CordobaCiencia @IUNAN_UCO

Share your work on social media! *EurJIC* has added Twitter as a means to promote your article. Twitter is an online microblogging service that enables its users to send and read short messages and media, known as tweets. Please check the pre-written tweet in the galley proofs for accuracy. If you, your team, or institution have a Twitter account, please include its handle @username. Please use hashtags only for the most important keywords, such as #catalysis, #nanoparticles, or #proteindesign. The ToC picture and a link to your article will be added automatically, so the **tweet text must not exceed 250 characters**. This tweet will be posted on the journal's Twitter account (follow us @EurJIC) upon publication of your article in its final (possibly unpaginated) form. We recommend you to re-tweet it to alert more researchers about your publication, or to point it out to your institution's social media team.

ORCID (Open Researcher and Contributor ID)

Please check that the ORCID identifiers listed below are correct. We encourage all authors to provide an ORCID identifier for each coauthor. ORCID is a registry that provides researchers with a unique digital identifier. Some funding agencies recommend or even require the inclusion of ORCID IDs in all published articles, and authors should consult their funding agency guidelines for details. Registration is easy and free; for further information, see http://orcid.org/.

Jorge de Haro
Prof. Álvaro Caballero http://orcid.org/0000-0002-2084-0686
Julián Morales
Dr. Almudena Benítez